The Sloshing Motion of Cross-Waves

By Jianke Yang

1. Introduction

Cross-waves are standing waves whose crests are perpendicular to a wavemaker. They have a frequency equal to half that of the wavemaker and can be generated in a wave tank when the wavemaker's frequency is near a subharmonic resonance (twice the natural frequency of a cross-wave mode), provided the forcing is strong enough to overcome dissipative effects. These waves were first reported by Michael Faraday in 1831. In his diary for July 1, 1831, Faraday observed that when a vibrating vertical plate was dipped into a basin of water, "Elevations, waves or crispations immediately formed but of a peculiar character ... beginning at the plate and projecting directly out from it ... like the teeth of a very short comb." He also remarked that these waves had a frequency half that of the excitation. The generating mechanism of these waves remained a mystery until 1970, when Garrett [1] found that a rectangular channel of finite length can be described by Mathieu's equation. Mahony [2] extended the analysis to a rectangular channel of infinite length. He found that the resonant bandwidth is an order of magnitude smaller than that in a channel of finite length. He also indicated that nonlinear effects may control the decay of the cross-waves down the channel. Using multiple-scale perturbation methods, Jones [3] first derived the governing

Address for correspondence: Prof. Jianke Yang, Department of Mathematics and Statistics, #401, University of Vermont, Burlington, VT 05401.

STUDIES IN APPLIED MATHEMATICS 95:171–191

Published by Blackwell Publishers, 238 Main Street, Cambridge, MA 02142, USA, and 108 Cowley Road, Oxford, OX4 1JF, UK.

nonlinear equations for the longitudinal modulation of a cross-wave mode in a rectangular channel of infinite length. These equations were later identified by Miles [4] as the nonlinear Schrödinger equation with a homogeneous wavemaker boundary condition and a null condition at infinity (referred to hereafter as the 2-D cross-wave equations). Using an averaged variational principle, Miles and Becker [5] obtained the same results as those of Jones. When the channel is wide enough to allow several adjacent cross-wave modes to be generated simultaneously, the cross-wave will also be modulated in the spanwise direction. Under the assumption that the spanwise modulation is much milder than the longitudinal one, so that the spanwise dispersion is negligible, the governing equations for both modulations were derived by Ayanle et al. [6] and hereafter are referred to as the (spanwisely nondispersive) 3-D cross-wave equations.

Experiments on cross-waves have been conducted by Barnard and Pritchard [7], Lichter and Shemer [8], Ayanle et al. [6], and Underhill et al. [9]. Barnard and Pritchard's [7] experiments demonstrated the generation of cross-waves in a long water channel. They also observed that "the cross-waves never reach a true state of equilibrium, and after the cross-wave amplitude has passed through a maximum, a wave detaches itself from the wavemaker, propagates along the channel," and eventually decays. These results were in agreement with Lichter and Chen's [10] numerical calculations of the 2-D cross-wave equations (when damping was incorporated). Miles and Becker [5], through analytical approximations and numerical integration, determined those stationary envelopes that are evanescent at large distances from the wavemaker. They compared their envelopes with Barnard and Pritchard's [7] experiments and Lichter and Chen's [10] numerical calculations, and suggested that stationary envelopes with either no or one maximum are stable for sufficiently small amplitudes and evolve into limit cycles for somewhat larger amplitudes. Ayanle et al. [6] observed a mixed-mode state. They then used a center manifold analysis on the 3-D cross-wave equations to reduce the PDEs to a system of coupled Landau equations in the neighborhood of a codimension–two point where two adjacent cross-wave modes are marginally stable. They found four possible steady states of the system, one of which is a mixed-mode superposition of two cross-wave modes. They predicted a Hopf bifurcation from the mixed mode for some parameters. Their experiments showed good agreement with the theoretical predictions. Underhill et al.'s [9] experiments revealed richer structures partially due to the presence of sloshing motion. They observed modulated, frequency-locked, and chaotic cross-waves in different regions of the parameter space. In particular, they observed that "at large cross-wave amplitudes, the spanwise wave structure apparently breaks up, because of modulational instability, into coherent soliton-like structures that propagate in the spanwise direction and are reflected by the sidewalls."

This paper studies two topics: (1) the general solution of the linearized cross-wave equations for an arbitrary initial condition, and (2) the dynamics of sloshing motion.

It is clear that the mechanism of cross-wave generation lies in the linearized 2-D cross-wave equations. The neutral curve, which sets the criterion as to when a cross-wave will be excited, should come from these linear equations. The cross-wave field characteristics along the channel at the initial stage of generation are also dictated by them. Therefore, knowledge of these equations' solution behaviors for an arbitrary initial condition is important. Previous research by Mahony [2] and Jones [3] found a special eigensolution of these linear equations. That solution was later used to establish the neutral curve. Such a neutral curve is apparently doubtful, and a resolution must be obtained from the solution for an arbitrary initial condition. In this paper, the analytical solution of the linearized 2-D cross-wave equations for an arbitrary initial condition is derived. The asymptotic behavior of this solution as time becomes large is given by simple formulas. These results fully describe the cross-wave field at its generating stage. The neutral curve based on this solution is also obtained. It is found that this neutral curve turns out to be the same as that based on the special eigensolution mentioned earlier.

Sloshing motion is an intriguing nonlinear phenomenon. It has been experimentally observed by Underhill et al. [9], but its dynamics is not yet known. Underhill et al. [9] speculated that it "may be related to the Benjamin–Feir instability of a uniform wave train." Since the Benjamin–Feir instability relies crucially on dispersion as well as on nonlinearity, this speculation emphasizes the importance of the spanwise dispersion, which is neglected in the 3-D cross-wave equations mentioned earlier. Doubts naturally arise at first sight, since in the present situation, two oppositely propagating wavetrains are involved, and the Benjamin–Feir instability of one uniform wavetrain may be irrelevant. This question is resolved because it can be proven that in deep water, each wavetrain still experiences the Benjamin–Feir instability in spite of the existence of the other. Serious doubts remain for the following reasons. First, the longitudinal modulation is coupled with the spanwise one and affects it in a nontrivial way. Second, and more important, the cross-wave field is nonconservative. The wavemaker transfers energy into this field and strongly affects its dynamics. Due to the nature of this problem, I propose in this paper that the spanwise dispersion does not play a major role; sloshing has a different nature from the Benjamin–Feir instability, and the dynamics of sloshing can be described by these (spanwisely nondispersive) 3-D cross-wave equations. To support this proposition, the solutions to these 3-D equations were studied. In view of the complexity of these nonlinear equations, numerical approaches were taken. The numerical results show various features of the cross-wave field. In particular, they show that, for a certain range of parameters, sloshing motion really appears. These sloshing waves propagate in the spanwise direction, are reflected by the sidewalls, and interact with each other in a persistent way. Due to the interaction of the sloshing and longitudinal waves, the motion of fluid particles is very complicated. All these results qualitatively agree well with Underhill et al.'s [9] observations on

sloshing motion, and give strong evidence of the connection between the sloshing motion and the 3-D cross-wave equations as well as the fact that the dynamics of sloshing is well described by these (spanwisely nondispersive) 3-D equations. Spanwise dispersion may be important to suppress very short waves, but it plays only a minor role in the dynamics of sloshing.

2. The analytical solution of the linearized 2-D cross-wave equations for an arbitrary initial condition

2.1. Formulation

Consider a rectangular semi-infinite water channel. The coordinates are such that $\tilde{x}$ ($\tilde{x} > 0$) measures distances along the channel, $\tilde{y}$ ($0 < \tilde{y} < b$) is the spanwise coordinate, and $\tilde{z}$ ($\tilde{z} < 0$) is depth below the free surface. Its driving mechanism is a wavemaker at $\tilde{x} = 0$, with the prescribed motion

$$\tilde{x} = a\tilde{f}(\tilde{z}) \sin 2\sigma\tilde{t} \qquad (\tilde{z} < 0), \tag{2.1}$$

where a is the maximum displacement of the wavemaker. The flow is assumed incompressible, inviscid, and irrotational. Dimensionless variables are defined using a as amplitude scale, g/σ^2 as length scale, and σ^{-1} as timescale, where g is the gravitational acceleration. Then the velocity potential ϕ and the surface displacement ζ are governed by the equations

$$\Delta\phi = 0, \tag{2.2}$$

$$\phi_z - \zeta_t = \epsilon(\phi_x\zeta_x + \phi_y\zeta_y) \qquad \text{on } z = \epsilon\zeta, \tag{2.3}$$

$$\phi_t + \zeta = -\frac{1}{2}\epsilon(\phi_x^2 + \phi_y^2) \qquad \text{on } z = \epsilon\zeta, \tag{2.4}$$

$$\phi \to 0 \qquad \text{as } z \to -\infty, \tag{2.5}$$

$$\phi_x - \epsilon f_z\phi_z \sin 2t = 2f(z)\cos 2t \qquad \text{on } x = \epsilon f(z)\sin 2t, \tag{2.6}$$

$$\phi_y = 0 \qquad \text{on } y = 0, l, \tag{2.7}$$

and also a radiation condition for large x. In these equations, $l = b\sigma^2/g$ and $\epsilon = a\sigma^2/g$.

We make the assumption that $\epsilon \ll 1$ (small-amplitude waves). At the first order, ϵ is put to be zero in equations (2.2)–(2.7). The solution to the resulting linear equations has two parts. The first part is expected—a progressive wave-train along the channel and a local standing disturbance around the wavemaker, both with the frequency 2. The second part is a free cross-wave mode with the frequency 1. This cross-wave may be excited through a kind of subharmonic resonance mechanism by the first part.

A free cross-wave mode with the frequency 1 and n transverse nodes has the velocity potential of the form

$$\phi_c = [A(X, T)e^{-it} + c.c.]\cos\frac{n\pi}{l}y\,e^z, \tag{2.8}$$

where $A(X, T)$ is the slowly varying complex amplitude, $X = \epsilon x$, and $T = \epsilon^2 t$. In order for this potential (2.8) to satisfy the Laplace equation (2.2) at the first order, it is required that $n\pi/l \approx 1$.

A multiple-scale perturbation method is used to determine the evolution equation of the cross-wave amplitude $A(X, T)$. It is found that A satisfies the following nonlinear 2-D cross-wave equations (see [3, 4]):

$$iA_T + \frac{1}{4}A_{XX} + \lambda A + \frac{1}{2}A^2A^* = 0, \tag{2.9}$$

$$A_X = iRA^* \qquad \text{on } X = 0, \tag{2.10}$$

$$A \longrightarrow 0 \qquad \text{as } X \longrightarrow \infty, \tag{2.11}$$

where

$$\lambda = \Lambda - 0.202G^2, \quad G = 4\int_{-\infty}^{0} f(z)e^{4z}\,dz, \quad \Lambda = \frac{1}{2\epsilon^2}\left(1 - \frac{n\pi}{l}\right) \tag{2.12}$$

and

$$R = \int_{-\infty}^{0} [4f(z) + f'(z)e^{2z}]\,dz - 2f(0). \tag{2.13}$$

The linearized 2-D cross-wave equations are

$$iA_T + \frac{1}{4}A_{XX} + \lambda A = 0, \tag{2.14}$$

$$A_X = iRA^* \qquad \text{on } X = 0, \tag{2.15}$$

$$A \longrightarrow 0 \qquad \text{as } X \longrightarrow \infty. \tag{2.16}$$

These linear equations govern the cross-wave field at its initial stage of generation.

As has been noted by Mahony [2] and Jones [3], the function

$$A(X, T) = e^{-2\sqrt{\lambda + i\sqrt{\frac{R^4}{16} - \lambda^2}}\,X + \sqrt{\frac{R^4}{16} - \lambda^2}\,T} \tag{2.17}$$

is a special eigensolution of the linear equations (2.14), (2.15), and (2.16) with the eigenvalue $\sqrt{R^4/16 - \lambda^2}$. Since this solution grows if $R^4/16 - \lambda^2 > 0$ and

is bounded if $R^4/16 - \lambda^2 < 0$, it has been conjectured that the neutral curve is $R^4/16 - \lambda^2 = 0$.

To clarify the neutral curve and to fully understand the cross-wave field behavior at its initial stage of generation, the solution of the equations (2.14), (2.15), and (2.16) for a general initial condition is required. In the next section, we set out to derive the analytical solution of those equations for an arbitrary initial condition

$$A|_{T=0} = A_0(X) \qquad (X \geq 0). \tag{2.18}$$

2.2. *Derivation of the analytical solution*

For convenience, the variables x and t are used instead of X and T in the rest of Section 2.

Rather than working with the real and imaginary parts of the complex amplitude A, here we work directly with A and A^*. Denoting $A^* \equiv B$, it is easy to find from (2.14), (2.15), and (2.16) that A and B satisfy the following equations:

$$\begin{aligned}
iA_t + \frac{1}{4}A_{xx} + \lambda A &= 0, \\
-iB_t + \frac{1}{4}B_{xx} + \lambda B &= 0,
\end{aligned}$$

$$\begin{aligned}
A_x &= iRB \qquad \text{on } x = 0, \\
B_x &= -iRA \qquad \text{on } x = 0,
\end{aligned}$$

$$\begin{aligned}
A &\longrightarrow 0 \qquad \text{as } x \longrightarrow \infty, \\
B &\longrightarrow 0 \qquad \text{as } x \longrightarrow \infty,
\end{aligned} \tag{2.19}$$

together with the initial conditions

$$\begin{aligned}
A_{t=0} &= A_0(x) \qquad (x \geq 0), \\
B_{t=0} &= B_0(x) \qquad (x \geq 0).
\end{aligned} \tag{2.20}$$

Note that $B_0(x) = A_0^*(x)$.

When Laplace transforms are taken for the equations (2.19) and (2.20) with respect to time t, A and B's Laplace transforms $\tilde{A}$, $\tilde{B}$ are found to satisfy the following equations:

$$\frac{1}{4}\tilde{A}_{xx} + (\lambda + is)\tilde{A} = iA_0(x), \tag{2.21}$$

$$\frac{1}{4}\tilde{B}_{xx} + (\lambda - is)\tilde{B} = -iB_0(x), \tag{2.22}$$

$$\tilde{A}_x = iR\tilde{B} \qquad \text{on } x = 0, \tag{2.23}$$

$$\tilde{B}_x = -iR\tilde{A} \qquad \text{on } x = 0, \tag{2.24}$$

$$\tilde{A} \longrightarrow 0 \qquad \text{as } x \longrightarrow \infty, \tag{2.25}$$

$$\tilde{B} \longrightarrow 0 \qquad \text{as } x \longrightarrow \infty. \tag{2.26}$$

The general solution of equation (2.21) is

$$\tilde{A}(x,s) = c_1 e^{-2\sqrt{-\lambda - is}\,x} + d_1 e^{2\sqrt{-\lambda - is}\,x} - \frac{i}{\sqrt{-\lambda - is}} \int_0^\infty A_0(x') e^{-2\sqrt{-\lambda - is}|x - x'|}\, dx', \tag{2.27}$$

where the complex function $\sqrt{-\lambda - is}$ has positive real part for s on the line $\mathrm{Re}(s) = \alpha_0 > 0$, α_0 is sufficiently large, and c_1, d_1 are complex constants.

Similarly, the general solution of (2.22) is

$$\tilde{B}(x,s) = c_2\, e^{-2\sqrt{-\lambda + is}x} + d_2\, e^{2\sqrt{-\lambda + is}\,x} + \frac{i}{\sqrt{-\lambda + is}} \int_0^\infty B_0(x') e^{-2\sqrt{-\lambda + is}|x - x'|}\, dx', \tag{2.28}$$

where the complex function $\sqrt{-\lambda + is}$ has positive real part for s on the line $\mathrm{Re}(s) = \alpha_0 > 0$, and c_2, d_2 are complex constants.

When the boundary conditions (2.25) and (2.26) are applied to the solutions (2.27) and (2.28), it is concluded that

$$d_1 = d_2 = 0. \tag{2.29}$$

The wavemaker boundary conditions (2.23) and (2.24) are then applied to the solutions (2.27) and (2.28), and two equations to determine c_1 and c_2 are obtained,

$$2\sqrt{-\lambda - is}\, c_1 + iR\, c_2 = \frac{R}{\sqrt{-\lambda + is}} \int_0^\infty B_0(x') e^{-2\sqrt{-\lambda + is}x'}\, dx' - 2i \int_0^\infty A_0(x') e^{-2\sqrt{-\lambda - is}x'}\, dx', \tag{2.30}$$

$$iR\ c_1 - 2\sqrt{-\lambda + is}\, c_2 = -\frac{R}{\sqrt{-\lambda - is}} \int_0^\infty A_0(x') e^{-2\sqrt{-\lambda - is}x'}\, dx' - 2i \int_0^\infty B_0(x') e^{-2\sqrt{-\lambda + is}x'}\, dx'. \tag{2.31}$$

c_1 and c_2 are found to be

$$c_1 = \frac{1}{R^2 - 4\sqrt{-\lambda - is}\sqrt{-\lambda + is}} \left\{ -4R \int_0^\infty B_0(x') e^{-2\sqrt{-\lambda+is}x'} \, dx' + \frac{i(4\sqrt{-\lambda+is}\sqrt{-\lambda-is} + R^2)}{\sqrt{-\lambda - is}} \int_0^\infty A_0(x') e^{-2\sqrt{-\lambda-is}x'} \, dx' \right\} \quad (2.32)$$

$$c_2 = \frac{1}{R^2 - 4\sqrt{-\lambda - is}\sqrt{-\lambda + is}} \left\{ -4R \int_0^\infty A_0(x') e^{-2\sqrt{-\lambda-is}x'} \, dx' - \frac{i(4\sqrt{-\lambda-is}\sqrt{-\lambda+is} + R^2)}{\sqrt{-\lambda + is}} \int_0^\infty B_0(x') e^{-2\sqrt{-\lambda+is}x'} \, dx' \right\}. \quad (2.33)$$

It is clear that $\tilde{A}$ is now fully determined and is in the form

$$\tilde{A}(x, s) = c_1 e^{-2\sqrt{-\lambda-is}x} - \frac{i}{\sqrt{-\lambda - is}} \int_0^\infty A_0(x') e^{-2\sqrt{-\lambda-is}|x-x'|} \, dx', \quad (2.34)$$

where c_1 is given by (2.32). The original solution $A(x, t)$ is the inverse Laplace transform of $\tilde{A}(x, s)$

$$A(x, t) = \frac{1}{2\pi i} \int_L \tilde{A}(x, s) e^{st} \, ds, \quad (2.35)$$

where the integration path L is to the right-hand side of all the singularities of $\tilde{A}(x, s)$.

2.3. The asymptotic behavior of the analytical solution $A(x, t)$ for large time t

To determine $A(x, t)$'s large-time asymptotic behavior, $\tilde{A}(x, s)$'s singularities need to be examined.

First consider the $\lambda < 0$ case.

The solution (2.34) has two branch points at $s = \pm i\lambda$. To guarantee that the complex functions $\sqrt{-\lambda - is}$ and $\sqrt{-\lambda + is}$ have positive real parts on the integration path L, write

$$\sqrt{-\lambda - is} = e^{-\frac{1}{4}\pi i}\sqrt{s - i\lambda}, \quad (2.36)$$

$$\sqrt{-\lambda + is} = e^{\frac{1}{4}\pi i}\sqrt{s + i\lambda}. \quad (2.37)$$

The branch cuts of $\sqrt{s - i\lambda}$ and $\sqrt{s + i\lambda}$ are located as shown in Figure 1.

Then define

$$\begin{aligned}
&\arg(s^+ - i\lambda) = \pi \quad \text{for } s^+ \text{ on the upper side of } \sqrt{s - i\lambda} \text{ cut;}\\
&\arg(s^- - i\lambda) = -\pi \quad \text{for } s^- \text{ on the lower side of } \sqrt{s - i\lambda} \text{ cut;}\\
&\arg(s^+ + i\lambda) = \pi \quad \text{for } s^+ \text{ on the upper side of } \sqrt{s + i\lambda} \text{ cut;}\\
&\arg(s^- + i\lambda) = -\pi \quad \text{for } s^- \text{ on the lower side of } \sqrt{s + i\lambda} \text{ cut.}
\end{aligned} \tag{2.38}$$

When (2.36) and (2.37) are introduced into equations (2.32) and (2.34), $\tilde{A}$ and c_1 can be rewritten in the following forms:

$$\begin{aligned}
\tilde{A}(x, s) &= c_1 e^{-2e^{-\frac{\pi i}{4}}\sqrt{s-i\lambda}x}\\
&\quad + \frac{e^{-\frac{\pi i}{4}}}{\sqrt{s - i\lambda}} \int_0^\infty A_0(x') e^{-2e^{-\frac{\pi i}{4}}\sqrt{s-i\lambda}|x-x'|}\, dx',
\end{aligned} \tag{2.39}$$

$$\begin{aligned}
c_1 = \frac{1}{R^2 - 4\sqrt{s - i\lambda}\sqrt{s + i\lambda}} &\left\{ -4R \int_0^\infty A_0^*(x') e^{-2e^{\frac{\pi i}{4}}\sqrt{s+i\lambda}x'}\, dx' \right.\\
&- \frac{e^{-\frac{\pi i}{4}}(4\sqrt{-\lambda + is}\sqrt{-\lambda - is} + R^2)}{\sqrt{s - i\lambda}}\\
&\left. \times \int_0^\infty A_0(x') e^{-2e^{-\frac{\pi i}{4}}\sqrt{s-i\lambda}x'}\, dx' \right\}.
\end{aligned} \tag{2.40}$$

Since

$$\frac{1}{R^2 - 4\sqrt{s - i\lambda}\sqrt{s + i\lambda}} = \frac{R^2 + 4\sqrt{s - i\lambda}\sqrt{s + i\lambda}}{16\left(\frac{R^4}{16} - \lambda^2 - s^2\right)}, \tag{2.41}$$

it is clear that $c_1(s)$ has poles at points

$$s = \pm\sqrt{\frac{R^4}{16} - \lambda^2}. \tag{2.42}$$

Making use of (2.41), c_1 can be expressed as

$$c_1(s) \equiv \frac{F(s)}{s^2 - \left(\frac{R^4}{16} - \lambda^2\right)} = \frac{F(s)}{\left(s - \sqrt{\frac{R^4}{16} - \lambda^2}\right)\left(s + \sqrt{\frac{R^4}{16} - \lambda^2}\right)}, \tag{2.43}$$

where

$$F(s) = \frac{(R^2 + 4\sqrt{s - i\lambda}\sqrt{s + i\lambda})}{16}\left\{4R\int_0^\infty A_0^*(x')e^{-2e^{\frac{\pi i}{4}}\sqrt{s+i\lambda}x'}\,dx'\right.$$
$$+ \frac{e^{-\frac{\pi i}{4}}(4\sqrt{-\lambda + is}\sqrt{-\lambda - is} + R^2)}{\sqrt{s - i\lambda}}$$
$$\left.\times\int_0^\infty A_0(x')e^{-2e^{-\frac{\pi i}{4}}\sqrt{s-i\lambda}x'}\,dx'\right\}. \tag{2.44}$$

Note that integrals such as

$$\int_0^\infty A_0(x')e^{-2e^{-\frac{\pi i}{4}}\sqrt{s-i\lambda}x'}\,dx'$$

do not contribute new singularities other than the branch points of $\sqrt{s - i\lambda}$ and $\sqrt{s + i\lambda}$, and they are less singular than $1/\sqrt{s - i\lambda}$ or $1/\sqrt{s + i\lambda}$ because $A_0(x)$ tends to zero as $x \longrightarrow \infty$, so $F(s)$ has no singularities other than the branch points of $\sqrt{s - i\lambda}$ and $\sqrt{s + i\lambda}$, and these singularities are weaker than $1/s - i\lambda$ or $1/s + i\lambda$. Similarly, the second term in (2.39) has no singularities other than the branch point of $\sqrt{s - i\lambda}$, and the singularity is weaker than $1/s - i\lambda$.

The above results on $\tilde{A}(x, s)$ are now used to determine the large-time asymptotic behaviors of $A(x, t)$. They are distinctively different depending on the sign of $R^4/16 - \lambda^2$.

1. $R^4/16 - \lambda^2 > 0$. In this case, the two simple poles $s = \pm\sqrt{R^4/16 - \lambda^2}$ are on the real axis. We choose an alternative integration path L′, as in Figure 2, and then use the residue theorem. After some simple asymptotic analysis, it is found that

$$A(x, t) \longrightarrow \frac{F\left(\sqrt{\frac{R^4}{16} - \lambda^2}\right)}{2\sqrt{\frac{R^4}{16} - \lambda^2}} e^{-2e^{-\frac{\pi i}{4}}\sqrt{\sqrt{\frac{R^4}{16}-\lambda^2}-i\lambda}x + \sqrt{\frac{R^4}{16}-\lambda^2}t} \quad \text{as } t \longrightarrow \infty. \tag{2.45}$$

This solution is exactly the same as the eigensolution noted by Mahony [2] and Jones [3]. It grows exponentially in time with the growth rate $\sqrt{R^4/16 - \lambda^2}$ and decays exponentially in the x direction.

2. $R^4/16 - \lambda^2 = 0$. In this case, $s = 0$ is a double pole. Choosing an alternative integration path L′ as in Figure 3 and performing a similar analysis, we find that

$$A(x, t) \longrightarrow [F(0)t + F'(0) + iF(0)|\lambda|^{-\frac{1}{2}}x]e^{-2|\lambda|^{\frac{1}{2}}x} \qquad \text{as } t \longrightarrow \infty. \tag{2.46}$$

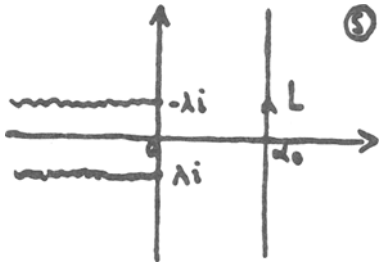

Figure 1. Branch cuts of $\sqrt{s - i\lambda}$ and $\sqrt{s + i\lambda}$.

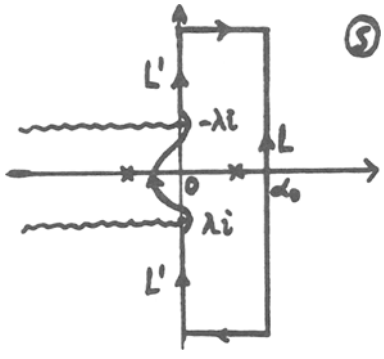

Figure 2. The alternative integration path L′ for the case $\frac{R^4}{16} - \lambda^2 > 0$.

This solution grows linearly in time and decays exponentially in the x direction.

3. $\frac{R^4}{16} - \lambda^2 < 0$. In this case, the two simple poles $s = \pm i\sqrt{\lambda^2 - R^4/16}$ are on the imaginary axis. When an alternative integration path L′ shown in Figure 4 is taken, a similar analysis reveals that

$$A(x,t) \longrightarrow \frac{F\left(i\sqrt{\lambda^2 - \frac{R^4}{16}}\right)}{2i\sqrt{\lambda^2 - \frac{R^4}{16}}} e^{-2e^{-\frac{\pi i}{4}}\sqrt{i\sqrt{\lambda^2-\frac{R^4}{16}}-i\lambda}\, x + i\sqrt{\lambda^2-\frac{R^4}{16}}\, t}$$

$$- \frac{F\left(-i\sqrt{\lambda^2 - \frac{R^4}{16}}\right)}{2i\sqrt{\lambda^2 - \frac{R^4}{16}}} e^{-2e^{-\frac{\pi i}{4}}\sqrt{-i\sqrt{\lambda^2-\frac{R^4}{16}}-i\lambda}\, x - i\sqrt{\lambda^2-\frac{R^4}{16}}\, t}$$

$$\text{as } t \longrightarrow \infty. \tag{2.47}$$

This solution is bounded for all time and decays exponentially in the x direction.

Now the case $\lambda \geq 0$ is discussed briefly.

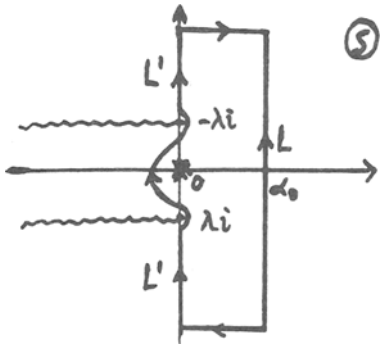

Figure 3. The alternative integration path L′ for the case $\frac{R^4}{16} - \lambda^2 = 0$.

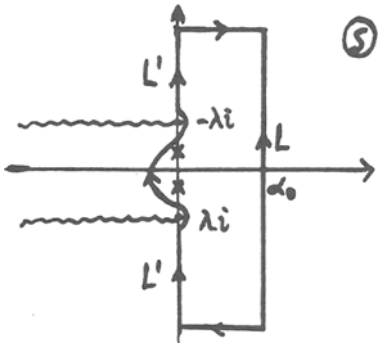

Figure 4. The alternative integration path L′ for the case $\frac{R^4}{16} - \lambda^2 < 0$.

Using previous arguments, it is found that the asymptotic solution always decays exponentially in the x direction.

1. When $R^4/16 - \lambda^2 > 0$, it grows exponentially in time and is the same as (2.45).
2. When $R^4/16 - \lambda^2 < 0$, it is bounded for all time and is the same as (2.47).
3. When $R^4/16 - \lambda^2 = 0$, the analysis is more complicated, but no new features appear.

2.4. The neutral curve

It is now clear that the neutral curve is $R^4/16 - \lambda^2 = 0$. It is reassured that the result is the same as that obtained based only on the special eigensolution (2.17) of the linearized 2-D cross-wave equations (2.14), (2.15), and (2.16). If $R^4/16 - \lambda^2 > 0$, the growth rate of the cross-wave is $\sigma = \sqrt{R^4/16 - \lambda^2}$.

When dissipation is modeled into the linearized 2-D cross-wave equation (2.14), it becomes

$$iA_t + \frac{1}{4}A_{xx} + (\lambda + iL)A = 0, \tag{2.48}$$

where $L > 0$ is linear damping constant. The boundary conditions (2.15) and (2.16) remain the same.

In this case, since the transformation $A = \hat{A}e^{-Lt}$ reduces this problem to the previous one, the analytical solution and its asymptotic form are just the undamped ones (as previously given) multiplied by e^{-Lt}. The neutral curve now becomes

$$\sqrt{\frac{R^4}{16} - \lambda^2} - L = 0. \tag{2.49}$$

3. Sloshing motion and the nonlinear 3-D cross-wave equations

3.1. Formulation

Consider a rectangular water channel of semi-infinite length ($\tilde{x} \geq 0$), infinite depth ($\tilde{z} \leq 0$), and finite width ($0 \leq \tilde{y} \leq b$). It is driven by a wavemaker at $\tilde{x} = 0$ at frequency 2σ. The generated cross-wave has the primary wavenumber $k_0 = N\pi/b$, where N is the number of transverse nodes. We assume that the channel is wide and N is large, but $k_0 = N\pi/b$ remains of order σ^2/g, where g is the gravitational acceleration. This cross-wave is modulated in both longitudinal and transverse directions.

Introduce the small perturbation parameter $\epsilon = N^{-\frac{1}{2}}$, and suppose that the motion of the wavemaker is prescribed by

$$\tilde{x} = \frac{\epsilon g}{\sigma^2}\tilde{f}(\tilde{z})\sin 2\sigma\tilde{t} \qquad (\tilde{z} < 0). \tag{3.1}$$

Dimensionless variables are defined using $\epsilon g/\sigma^2$ as amplitude scale, g/σ^2 as length scale, and σ^{-1} as timescale. The velocity potential ϕ and the surface displacement ζ are governed by the equations (2.2) to (2.7), together with a radiation condition for large x.

The velocity potential for the cross-wave is of the form

$$\phi_c = \left[A(X, Y, T)e^{i(\frac{k_0}{k}y+t)} + B(X, Y, T)e^{i(\frac{k_0}{k}y-t)} + c.c.\right]e^z, \tag{3.2}$$

where

$$k = \frac{\sigma^2}{g}, \qquad X = \epsilon x, \qquad Y = \epsilon^2\frac{k_0}{k}y \qquad \text{and } T = \epsilon^2 t. \tag{3.3}$$

A multiple-scale perturbation analysis results in the following equations for A and B (see [6]):

$$-iA_T + \frac{1}{4}A_{XX} + \frac{1}{2}iA_Y + (J - iL)A - 2|A|^2A + 4|B|^2A = 0,$$
$$iB_T + \frac{1}{4}B_{XX} + \frac{1}{2}iB_Y + (J + iL)B - 2|B|^2B + 4|A|^2B = 0,$$

$$\begin{aligned} A_X &= iRB \qquad \text{on } X = 0, \\ B_X &= -iRA \qquad \text{on } X = 0, \\ A &= B^* \qquad \text{on } Y = 0, \pi, \end{aligned}$$

$$\begin{aligned} A &\longrightarrow 0 \qquad \text{as } X \longrightarrow \infty, \\ B &\longrightarrow 0 \qquad \text{as } X \longrightarrow \infty, \end{aligned} \tag{3.4}$$

where

$$J = \Lambda - 0.202G^2, \quad G = 4\int_{-\infty}^{0} f(z)e^{4z}\,dz, \quad \Lambda = \frac{1}{2\epsilon^2}\left(1 - \frac{k_0}{k}\right), \tag{3.5}$$

$$R = \int_{-\infty}^{0} [4f(z) + f'(z)e^{2z}]\,dz - 2f(0), \tag{3.6}$$

and $L > 0$ is a linear damping constant. With the introducion of new scalings

$$\begin{aligned} \bar{X} &= \sqrt{2}X, \qquad \bar{Y} = Y, \qquad \bar{T} = \tfrac{1}{2}T, \\ \bar{A} &= 2A, \qquad \bar{B} = 2B, \qquad \bar{R} = \tfrac{1}{\sqrt{2}}R, \end{aligned} \tag{3.7}$$

and the bars dropped, the following system of equations for the complex amplitudes A and B of the cross-waves is obtained:

$$-iA_T + A_{XX} + iA_Y + (J - iL)A - |A|^2A + 2|B|^2A = 0, \tag{3.8}$$
$$iB_T + B_{XX} + iB_Y + (J + iL)B - |B|^2B + 2|A|^2B = 0, \tag{3.9}$$

$$A_X = iRB \qquad \text{on } X = 0, \tag{3.10}$$
$$B_X = -iRA \qquad \text{on } X = 0, \tag{3.11}$$
$$A = B^* \qquad \text{on } Y = 0, \pi, \tag{3.12}$$

$$A \longrightarrow 0 \qquad \text{as } X \longrightarrow \infty, \tag{3.13}$$

$$B \longrightarrow 0 \qquad \text{as } X \longrightarrow \infty. \tag{3.14}$$

Note that in the above derivation, spanwise modulations are assumed to be an order of magnitude weaker than longitudinal ones so that spanwise dispersion is negligible.

3.2. The analytical solution of the linearized 3-D cross-wave equations for an arbitrary initial condition

At the initial stage of cross-wave generation, A and B are both very small. So they are governed by the linearized 3-D cross-wave equations, namely,

$$-iA_T + A_{XX} + iA_Y + (J - iL)A = 0, \tag{3.15}$$

$$iB_T + B_{XX} + iB_Y + (J + iL)B = 0, \tag{3.16}$$

$$A_X = iRB \qquad \text{on } X = 0, \tag{3.17}$$

$$B_X = -iRA \qquad \text{on } X = 0, \tag{3.18}$$

$$A = B^* \qquad \text{on } Y = 0, \pi, \tag{3.19}$$

$$A \longrightarrow 0 \qquad \text{as } X \longrightarrow \infty, \tag{3.20}$$

$$B \longrightarrow 0 \qquad \text{as } X \longrightarrow \infty. \tag{3.21}$$

It has been shown that in this case, A and B can be written as a linear eigenmode expansion of the form [6]

$$A = \sum_{k=-\infty}^{\infty} A_k(X, T)e^{ikY}, \tag{3.22}$$

$$B = \sum_{k=-\infty}^{\infty} A_k^*(X, T)e^{ikY}, \tag{3.23}$$

and A_k^* is governed by the equations

$$iA_{kT}^* + A_{kXX}^* + (J - k + iL)A_k^* = 0,$$

$$A_{kX}^* = -iRA_k \qquad \text{on } X = 0,$$

$$A_k^* \longrightarrow 0 \qquad \text{as } X \longrightarrow \infty. \tag{3.24}$$

These equations are the same as equations (2.48), (2.15), and (2.16), so the analytical solution for A_k^* and its asymptotic behavior are obtained as before. Therefore the analytical solutions for A and B can be constructed from the relations (3.22) and (3.23). The k-th cross-wave mode is excited if $\sqrt{R^4 - (J-k)^2} - L > 0$. If the forcing is strong, i.e., if R is sufficiently large, several adjacent cross-wave modes are generated, and large-scale spanwise modulations are to be expected.

3.3. Numerical methods for the nonlinear 3-D cross-wave equations

Sloshing motion is, without doubt, a nonlinear phenomenon, but the role of spanwise dispersion is unclear. If this dispersion is crucial, sloshing appears related to the Benjamin–Feir instability of a uniform wavetrain. But this may not be the case. In view of the special nature of the cross-waves, it is proposed here that the spanwise dispersion plays a minor role and that the dynamics of sloshing can be described by the (spanwisely nondispersive) 3-D cross-wave equations (3.8)–(3.14). To verify this conjecture, numerical methods are developed for these equations, and numerical calculations are subsequently carried out.

The nonlinear 3-D cross-wave equations (3.8)–(3.14) are first divided into real and imaginary parts and equations with respect to Re(A), Im(A), Re(B), and Im(B) are derived. These equations are solved numerically by an explicit finite difference scheme which uses second-order central difference operators to approximate spatial derivatives

$$\partial_{XX} \longrightarrow \delta_{XX}, \qquad \partial_Y \longrightarrow \delta_Y^2, \tag{3.25}$$

and the fourth-order Runge–Kutta scheme to advance in time. The boundary conditions at the wavemaker $X = 0$ and at the sidewalls $Y = 0, \pi$ are also approximated by second order difference operators, which use the boundary point and two adjacent points in the domain. A sufficiently large interval for X is used so that the outer boundary condition for X can be taken as $A = B = 0$.

The adopted scheme is consistent, and its truncation error is second order in space and fourth order in time. The stability condition restricts the size of the time step. The determination of the computational step-sizes is based on experience with testing the code as well as on stability and accuracy concerns.

The initial conditions were chosen to be

$$A_0(X, Y) = e^{-RX}[a_1(1-i) + a_2(1+i)Y(Y-\pi)], \tag{3.26}$$

and

$$B_0(X, Y) = e^{-RX}[a_1(1+i) - a_2(1-i)Y(Y-\pi)], \tag{3.27}$$

which satisfy the boundary conditions (3.10)–(3.14). The real constants a_1 and a_2 were chosen as $a_1 = a_2 = 0.05$ in the actual runs and $a_1 = a_2 = 0.005$ in the code testing.

The code was tested against the linear analytical solution for the case with parameters $R = 1.6$, $J = 0$, and $L = 2$. The domain was bounded by $0 \leq X \leq 7$, $0 \leq Y \leq \pi$, and $0 \leq T \leq 6$. The step sizes were chosen as $\Delta X = 0.05$, $\Delta Y = \pi/80 \approx 0.04$, and $\Delta T = 0.0003$. $a_1 = a_2 = 0.005$ was taken in the initial conditions (3.26) and (3.27). The comparison showed excellent agreement between the numerical and analytical solutions.

3.4. Numerical results and sloshing motion

Many runs with different parameters have been carried out in detail. The results are basically similar to the ones shown in this paper with parameters $R = 1.6$, $J = -0.5$, and $L = 1.6$. The domain was defined by $0 \leq X \leq 7$, $0 \leq Y \leq \pi$, and $0 \leq T \leq 12$. The step sizes were chosen to be $\Delta X = 0.07$, $\Delta Y = \pi/80 \approx 0.04$, and $\Delta T = 0.0003$. $a_1 = a_2 = 0.05$ was taken in the initial conditions (3.26) and (3.27).

The results are shown in Figures 5–8.

The following interesting features are emphasized:

1. Sloshing motion really appears, as can be seen in Figure 5. The cross-waves are excited first. They then become more localized spanwise, and sloshing motion begins to appear. These sloshing waves travel in the transverse direction, are reflected by the side walls, and interact with each other in a persistent way.
2. Due to the interaction of the sloshing and longitudinal waves, the motion of fluid particles is much more complicated than in cases without spanwise modulations (see Lichter and Chen's [10] computations of the 2-D cross-wave equations, etc.). This feature is clear in Figure 6.

Comparison with the relevant experimental results is interesting. Underhill et al. [9] observed that "at large cross-wave amplitudes, the noisy periodic states, consisting of two or more waves traversing the span of the tank, appeared. These waves became progressively more localized and appeared soliton-like as the forcing amplitude was increased." They were also "reflected by the sidewalls." These observations qualitatively agree well with the numerical calculations.

This agreement sheds some light on the dynamics of the sloshing motion. As the numerical results have shown, the sloshing waves can arise without including spanwise dispersion and are well described by the 3-D cross-wave equations (3.8)–(3.14). Therefore, it appears that sloshing motion bears little relationship to the Benjamin–Feir instability of a uniform wavetrain. Uniform spanwise, standing cross-waves break up, because of modulational instability, into transversely localized sloshing waves. This instability is due to the forcing of the wavemaker and the nature of the problem, not to the Benjamin–Feir instability.

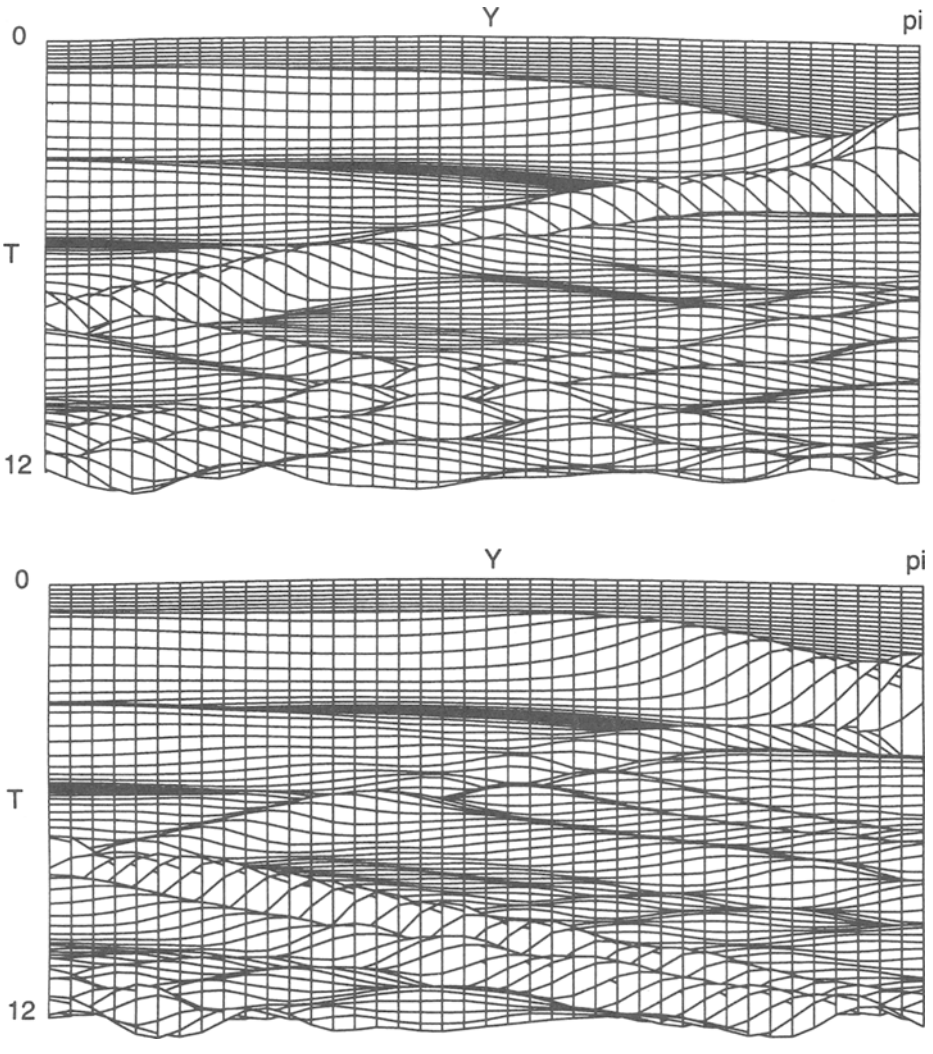

Figure 5. The time-evolution of the cross-waves at the wavemaker ($X = 0$). $0 \leq Y \leq \pi$, $0 \leq T \leq 12$. The upper panel is the $|A|$ plot, and the lower panel is the $|B|$ plot. Note that the sloshing waves are generated, and they then propagate across the span of the channel.

4. Summary

In this paper, the analytical solution was obtained for the linearized cross-wave equations with an arbitrary initial condition. This solution conclusively established the neutral curve and fully described the cross-wave field at the initial stages of its generation. The dynamics of the sloshing motion was explored, and the connection between the sloshing motion and the (spanwise nondispersive)

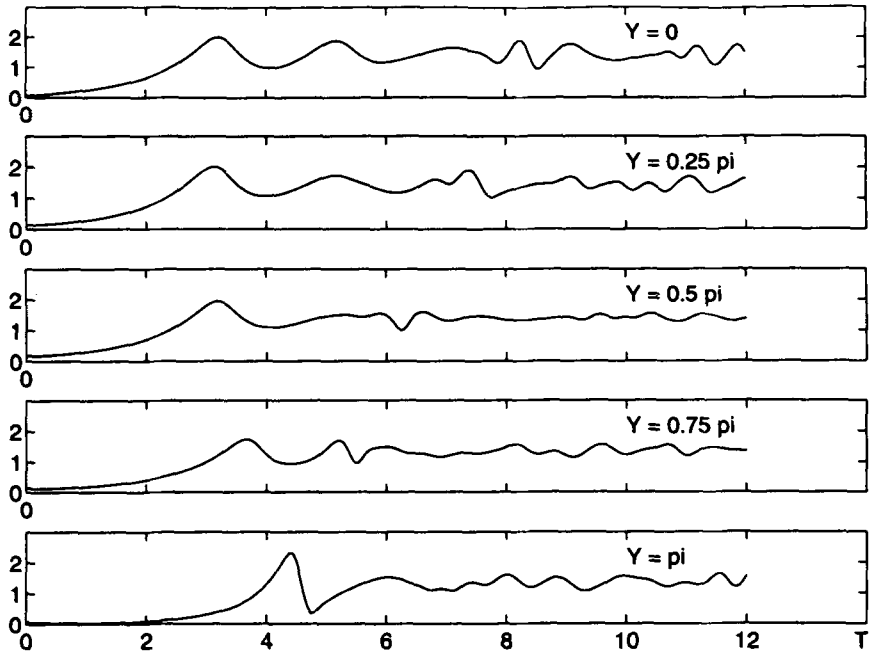

Figure 6. The time-evolution of the cross-waves at the following positions: $(X, Y) = (0, 0), (0, \frac{\pi}{4}), (0, \frac{\pi}{2}), (0, \frac{3\pi}{4})$, and $(0, \pi)$. Only $|A|$ is plotted. $|B|$ is quite similar. $0 \leq T \leq 12$.

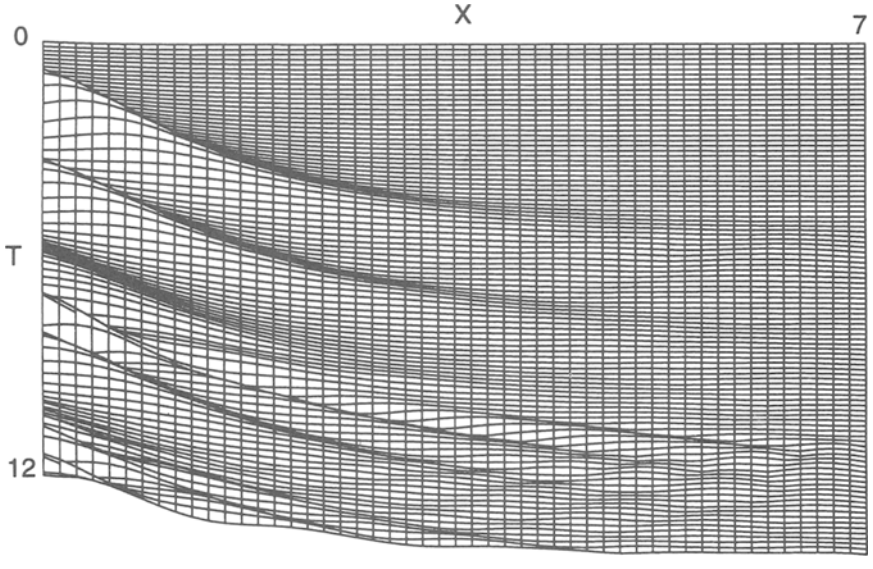

Figure 7. The time-evolution of the cross-waves at one sidewall ($Y = 0$). $0 \leq X \leq 7$, $0 \leq T \leq 12$. Only $|A|$ is plotted. $|B|$ is quite similar.

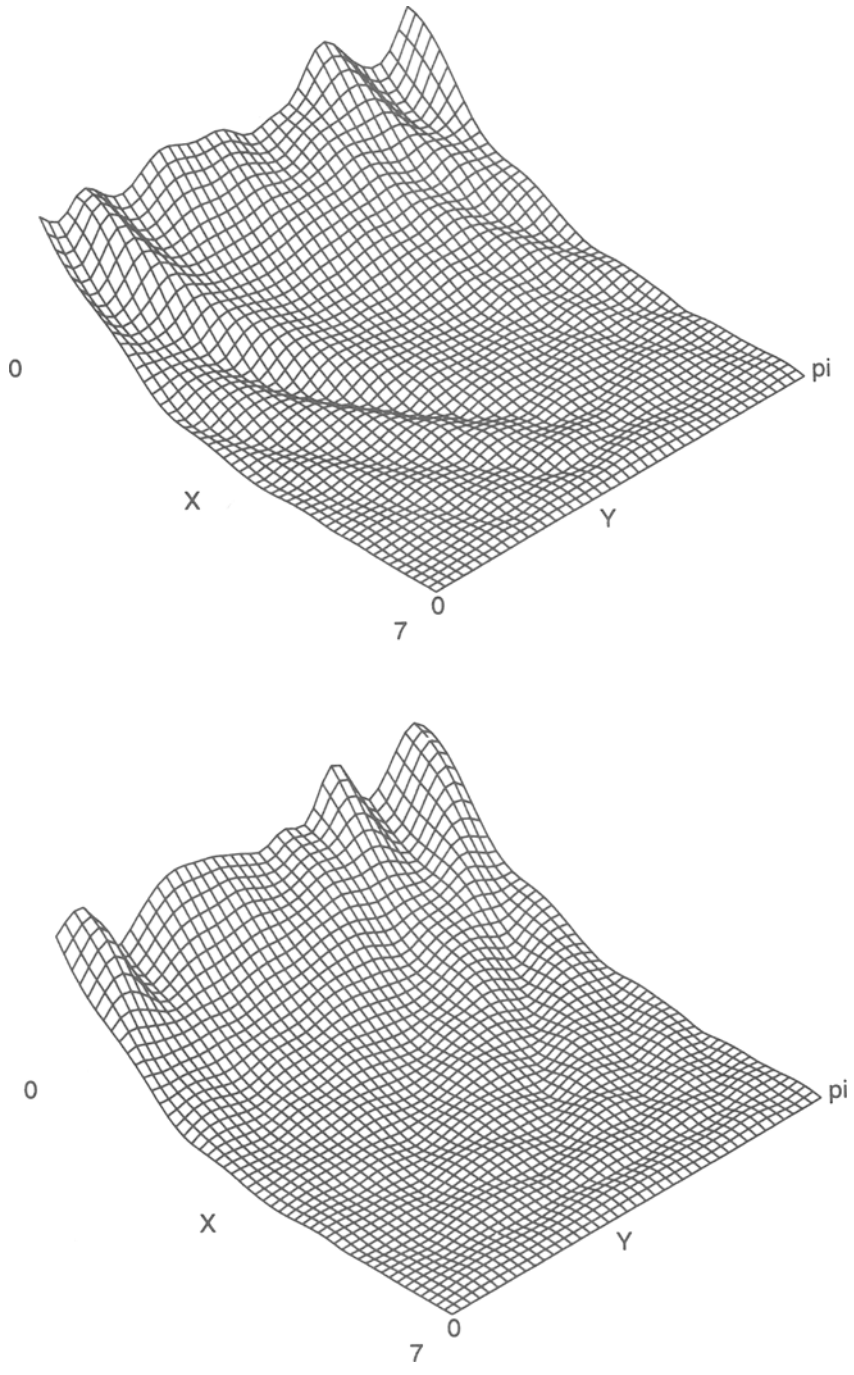

Figure 8. The cross-wave field at the time $T = 12$. $0 \leq X \leq 7$, $0 \leq Y \leq \pi$. The upper panel is the $|A|$ plot, and the lower panel is the $|B|$ plot.

3-D cross-wave equations (3.8)–(3.14) has been established. The sloshing waves are due to a kind of modulational instability not related to the Benjamin–Feir instability of uniform wavetrains.

Acknowledgment

I would like to express my gratitude to Prof. D. J. Benney for his advice and constant encouragement during the course of this work.

References

1. C. J. R. GARRETT, *J. Fluid Mech.* 41:837–849 (1970).
2. J. J. MAHONY, *J. Fluid Mech.* 55:229–244 (1972).
3. A. F. JONES, *J. Fluid Mech.* 138:53–74 (1984).
4. J. W. MILES, *J. Fluid Mech.* 151:391–394 (1985).
5. J. MILES and J. BECKER, *J. Fluid Mech.* 186:129–146 (1988).
6. H. AYANLE, A. J. BERNOFF, and S. LICHTER, *Physica* D 43:87–104 (1990).
7. B. J. S. BARNARD and W. G. PRITCHARD, *J. Fluid Mech.* 55:245–255 (1972).
8. S. LICHTER and L. SHEMER, *Phys. Fluids* 29:3971–3975 (1986).
9. W. B. UNDERHILL, S. LICHTER, and A. J. BERNOFF, *J. Fluid Mech.* 225:371–394 (1991).
10. S. LICHTER and J. CHEN, *J. Fluid Mech.* 183:451–465 (1987).

UNIVERSITY OF VERMONT

(Received July 14, 1994)